Supporting Information for:

Intramolecular Hydrogen Bonding Facilitates Electrocatalytic Reduction of Nitrite in Aqueous Solution

Song Xu, Hyuk-Yong Kwon, Daniel C. Ashley, Chun-Hsing Chen, Elena Jakubikova, Jeremy M. Smith

Table of Contents

Experimental and Supplementary Figures

General Considerations

All anaerobic manipulations, including non-aqueous electrochemical measurements, were performed under a nitrogen atmosphere using standard Schlenk techniques or in an MBraun Labmaster glovebox. Deionized water was used for all aqueous experiments or measurements. All reagents were purchased from commercial venders and used as received. $[Co(DIM)Br_2]^+$ and $[Co(DIM)(NO_3)_2]^+$ (DIM = 2,3-dimethyl-1,4,8,11-tetraazacyclotetradeca-1,3-diene) were prepared according to literature procedures.[1-2] ^1H NMR data were recorded on a Varian Inova 400 MHz spectrometer at 22 ºC. UV-visible spectra were recorded with an Agilent Cary 60 UV-visible spectrometer. Mass spectra were recorded using positive electrospray ionization on a Thermo Electron Corp MAT-95XP spectrometer. Solution magnetic susceptibilities were determined by Evans method.[3]

Characterization of Nitrite Reduction Products

Ammonia and hydroxylamine after bulk electrolysis are characterized according to literature procedures.[4-5] For a typical experiment to characterize NH_3: 5 mL of reagent A (500 mL aqueous solution of 5 g phenol plus 25 mg sodium nitroprusside) and 100 μL of sample solution are added into a test tube. After the tube is vigorously shaken, 5 mL of reagent B (500 mL aqueous solution of 2.5 g NaOH and 4.2 mL of sodium hypochlorite) is added into the solution. The color of the solution is developed at 37 °C for 20 minutes and the absorbance at 625 nm measured at room temperature. A calibration curve for ammonia quantification is constructed using standard ammonium sulfate solution . The amount of NH_3 after electrolysis is quantified according to tthis calibration curve. Control experiments reveal that color development does not occur in the

presence of any of the species present in the electrocatalysis experiments, i.e. catalyst, electrolyte, etc. The possible formation of NH_2OH was similarly tested for using following literature procedures,[5] however no absorption band is observed at *ca.* 700 nm, ruling out the formation of hydroxylamine.

Physical Methods

Cyclic voltammetry experiments in aqueous solution were carried out in an argon purged, air-tight, single compartment cell, while CV experiments in non-aqueous media were carried out in an MBraun Labmaster glovebox. Working electrode: glassy carbon electrode (3×3 mm^2, CH Instruments). Auxiliary electrode: platinum wire (Alfa Aesar, 99.99%). Pseudo-reference electrode: Ag wire (Alfa Asear, 99.99%) for non-aqueous and Ag/AgCl (CH Instruments, 1M KCl, -0.006 V vs SCE) for aqueous solutions. The final redox potentials measured under non-aqueous conditions were calculated by comparing the measured potentials with $E_{1/2}$ of Fc^+/Fc in the same solution then converted to potential vs SCE by adding 0.40 V.[6] The reproducibility of all cyclic voltammetry experiments are verified by several repeated scans. Average peak current densities calculated from multiple scans were used for quantitative kinetic studies.

Controlled-potential electrolysis (CPE) were carried out in a two-compartment cell separated by frit. Working electrode: carbon rod electrode (0.5 cm in diameter, 5 cm in length), auxiliary electrode: carbon rod electrode, reference electrode Ag/AgCl (CH Instruments, 1 M KCl, -0.006 V vs SCE). The solution after electrolysis at -1.05 V vs SCE for 2 hours was analyzed for NH_3, allowing the Faradaic efficiency and TON to be calculated.

Preparation of $[Co(DIM)(NO_2)_2](BPh_4)$: A 20 mL vial (wrapped with aluminum foil) was charged with $AgNO_2$ powder (46.2 mg, 0.3 mmol, 3.05 eq) and a solution of $[Co(DIM)Br_2]^+$ (50

mg, 0.096 mmol, 1 eq) in methanol (15 mL). The resulting solution of mixture was stirred in an ice bath for 2 h until the green solution changed to pale yellow. The off-white precipitate (AgBr) was removed through filtration and the pale yellow solution was collected. Solid $NaBPh_4$ (34.2 mg, 0.1 mol, 1.05 eq) was added, the methanol was removed *in vacuo* and the complex extracted with dichloromethane (20 mL). The dichloromethane was removed under reduced pressure to give a pale-yellow powder (28.0 mg, 41%). Crystals of $[Co(DIM)(NO_2)_2](BPh_4)$ suitable for single crystal X-ray diffraction were obtained by slow diffusion of diethyl ether into a dichloromethane solution of the complex. ^{1}H NMR (CD_3CN, 400 MHz): δ 6.21 (2H, br, NH_h); 3.92 (2H, d, $CH_{b/c}$); 3.82 (2H, t, $CH_{b/c}$); 2.95 (2H, m, $CH_{i/j}$); 2.79 (2H, d, $CH_{g/f}$); 2.79 (2H, m, $CH_{i/j}$); 2.58 (6H, s, CH_a); 2.45-2.55 (2H, d, $CH_{g/f}$); 2.32 (2H, d, $CH_{d/e}$), 1.99 (2H, d, $CH_{d/e}$). The ^{1}H NMR signals are assigned according to the NMR spectra of Figure S1 to S3. ESI-MS: calcd for $[Co(DIM)(NO_2)_2]^+$: ($C_{12}H_{24}CoN_6O_4$) m/z: 375.12 (M+); found: 375.1.

***In situ* generation of [Co(DIM)(NO$_2$)$_2$]Br:** A 20 mL vial was charged with $[Co(DIM)Br_2]^+$ (10.0 mg, 0.02 mmol, 1 eq), $NaNO_2$ (3.0 mg, 0.042 mmol, 2.1 eq) and CD_3OD (4 mL). The mixture was stirred in an ice bath for half hour until the green solution became yellow. The resulting CD_3OD solution was then directly characterized by ^{1}H NMR spectroscopy. The ^{1}H NMR spectrum in CD_3OD matches that of the isolated $[Co(DIM)(NO_2)_2]BPh_4$ complex (Figure S5).

Preparation of Co(DIM)(NO$_2$)$_2$: Under anaerobic conditions, cobaltocene (5.7 mg, 0.03 mmol, 1.05 eq) was added to a solution of $[Co(DIM)(NO_2)_2]BPh_4$ (20.0 mg, 0.028 mmol, 1 eq) in acetonitrile (10 mL). Upon addition, the color of solution immediately changed from pale yellow to dark purple. The reaction was stirred at room temperature overnight before being dried under reduced pressure to afford mixture of dark purple ($Co(DIM)(NO_2)_2$) and pale yellow ($[Cp_2Co]^+$) powders. The cobaltocenium salt could be partially removed by extensive washing with THF. Dark

purple crystals of $Co(DIM)(NO_2)_2$ suitable for single crystal X-ray diffraction were obtained by slow diffusion of diethyl ether into its dichloromethane solution. Approximate yield (with $[Cp_2Co]^+$ impurity): 4 mg, 35%. μ_{eff} = 1.73 μ_B. We were unable to obtain sufficient quantities of pure complex for analysis of bulk purity.

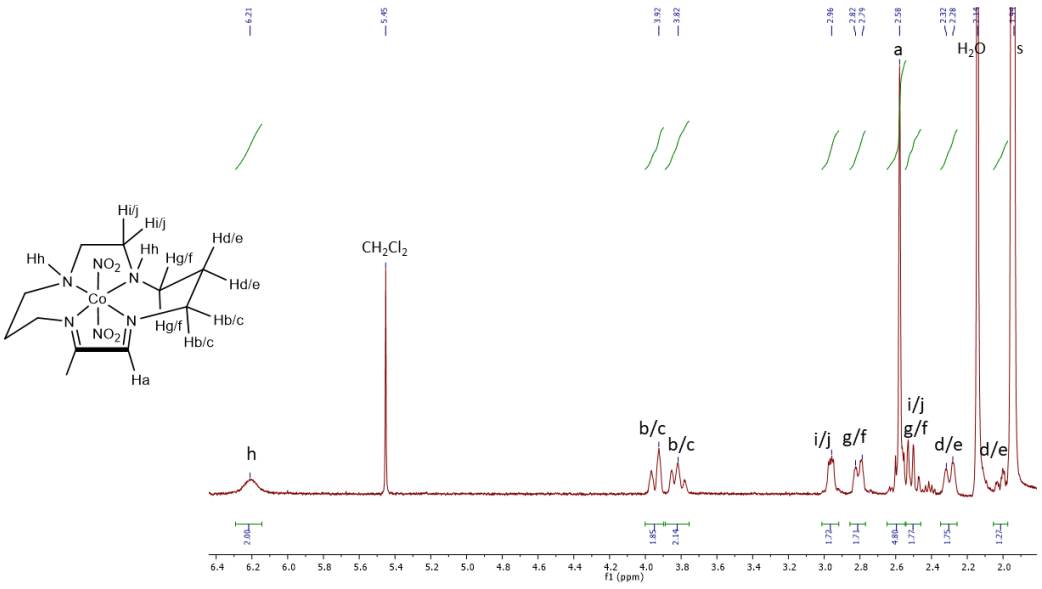

Figure S1. ^{1}H NMR spectrum of $[Co(DIM)(NO_2)_2]BPh_4$ (solvent: CD_2Cl_2) with peak assignments based on COSY, HSQC and spectra (Figure S2 and Figure S3), s = protio impurities in CD_3CN.

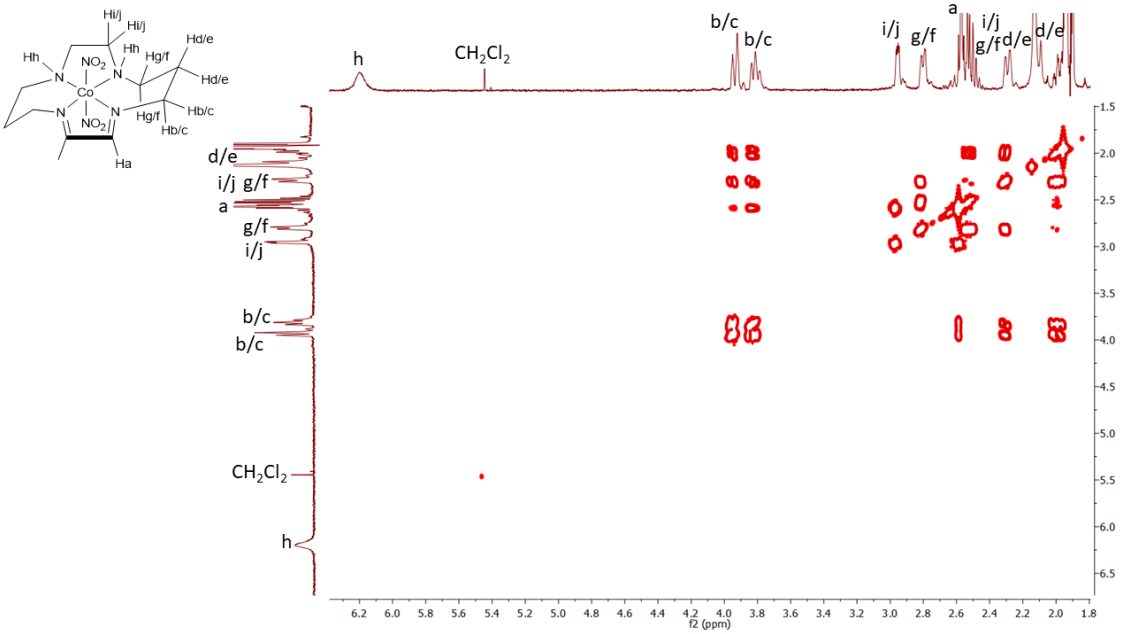

Figure S2. COSY NMR spectrum of $[Co(DIM)(NO_2)_2]^+$ (solvent: CD_2Cl_2), s = protio impurities in CD_3CN.

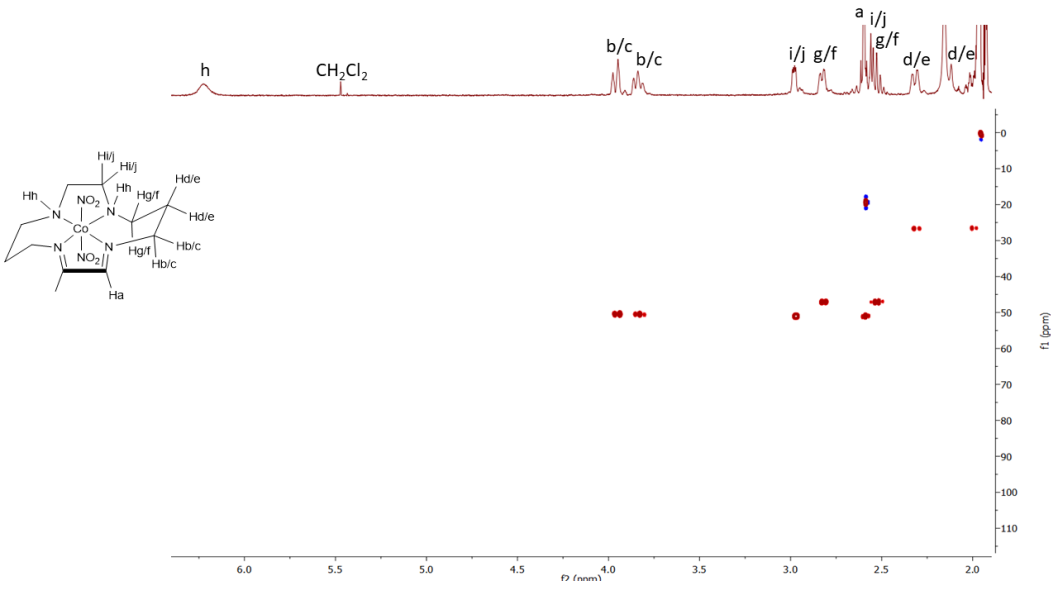

Figure S3. HSQC NMR spectrum of $[Co(DIM)(NO_2)_2]^+$ (solvent: CD_3CN), s = protio impurities in CD_3CN.

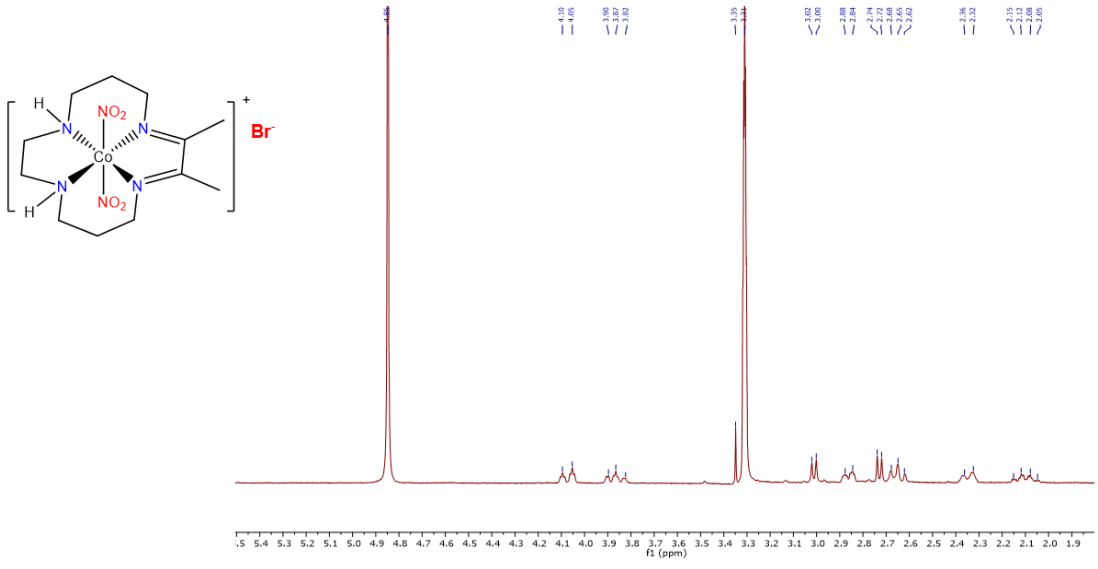

Figure S4. ^{1}H NMR spectrum of [Co(DIM)(NO$_2$)$_2$]Br prepared *in situ* prepared from [Co(DIM)Br$_2$]Br and 2eq of NaNO$_2$ (solvent: CD$_3$OD). The spectrum is the same as that of [Co(DIM)(NO$_2$)$_2$](BPh$_4$) in Figure S5 (top).

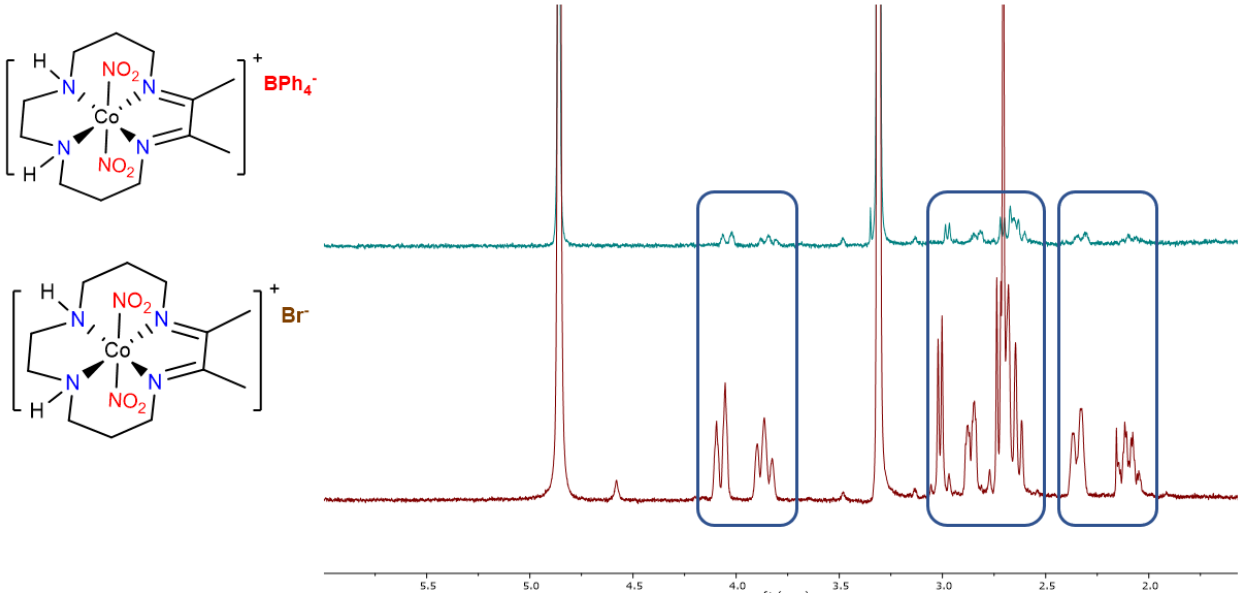

Figure S5. ^{1}H NMR spectrum of isolated [Co(DIM)(NO$_2$)$_2$](BPh$_4$) (top) and *in situ* generated [Co(DIM)(NO$_2$)$_2$]Br (bottom) (solvent: CD$_3$OD).

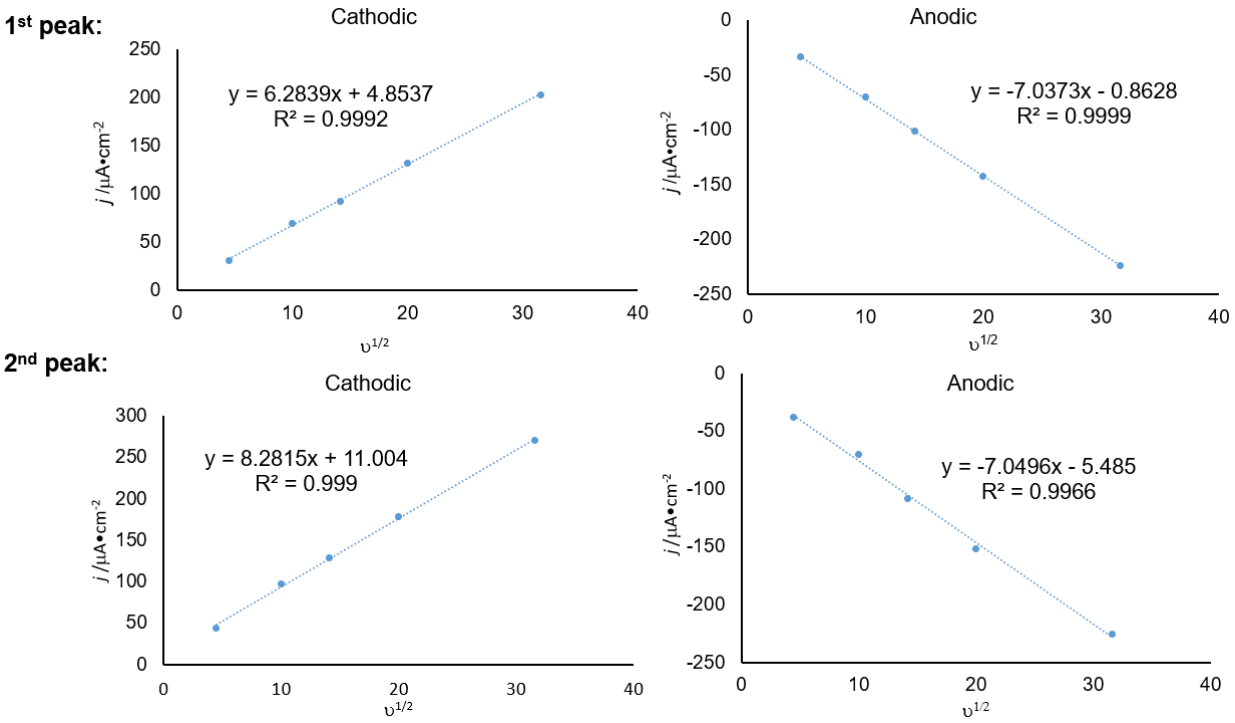

Figure S6. Dependence of peak current densities on the square root of the scan rate for the Co(III)/Co(II) and Co(II)-(DIM)/Co(II)-(DIM^{-1}) couples of [Co(DIM)(NO$_2$)$_2$]BPh$_4$ under nonaqueous condition. Linear dependencies are observed in both the cathodic and anionic directions, suggesting both redox processes in Figure 2 are electrochemically reversible.

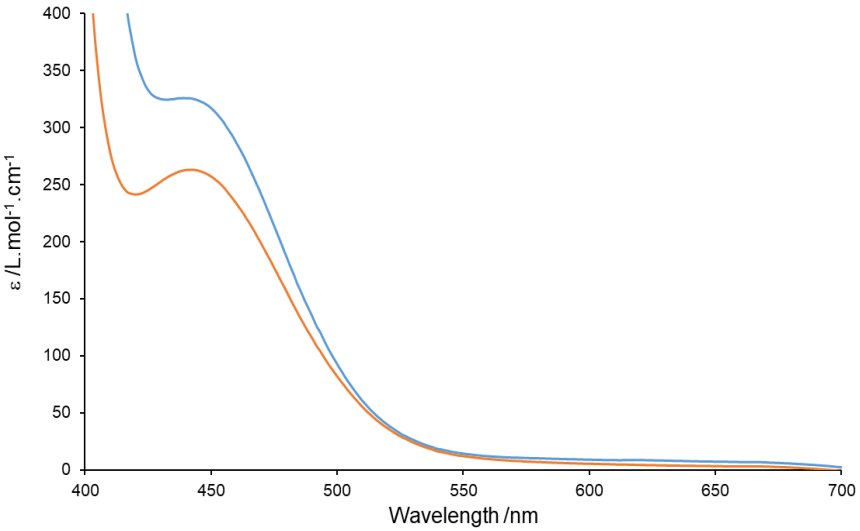

Figure S7. UV-vis spectra of 0.5 mM. $[Co(DIM)(NO_2)_2]BPh_4$ in MeCN (blue) and 0.5 mM $[Co(DIM)Br_2]^+$ with 100 mM $NaNO_2$ in H_2O (orange). The similarity of the UV-vis spectra support the *in situ* generation of $[Co(DIM)(NO_2)_2]^+$ in H_2O.

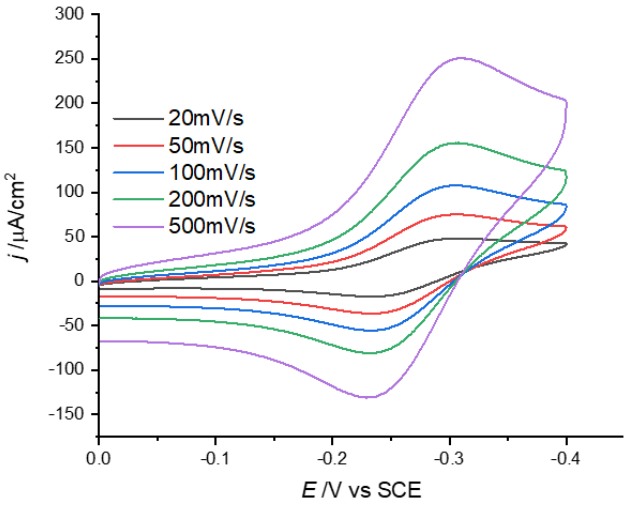

Figure S8. Cyclic voltammograms of 0.5 mM $[Co(DIM)Br_2]^+$ with 50 mM $NaNO_2$ under different scan rates. The reversibility observed in the cyclic voltammogram suggests the redox process observed at *ca.* -0.3 V vs SCE under aqueous condition is reversible in the presence of excess NO_2^- (Scheme 2).

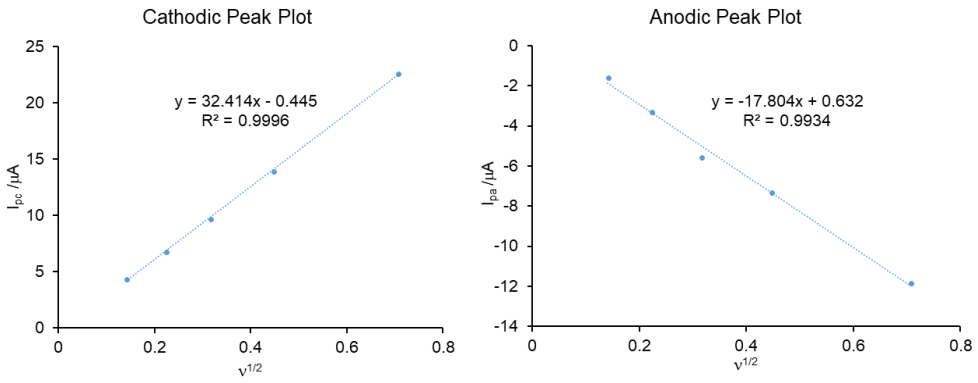

Figure S9. Dependence of peak current densities on the square root of the scan rate for the Co(III)/Co(II) couples of $[Co(DIM)Br_2]^+$ with excess $NaNO_2$ under aqueous condition (Figure 3a, Figure S8). Since linear dependences are observed in both the cathodic and anionic directions, the redox process is electrochemically reversible.

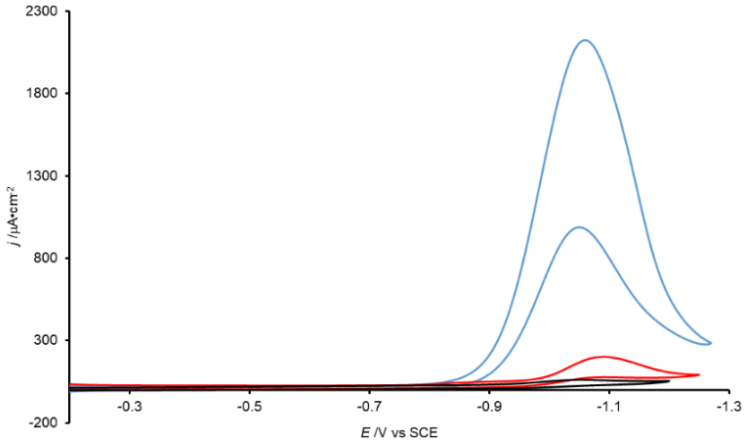

Figure S10. Cyclic Voltammogram of 0.5 mM $[Co(DIM)Br_2]^+$ without substrate (black), 10 mM $NaNO_3$ (red) and 10 mM $NaNO_2$ (blue) at pH = 6.3. Scan rate = 5 mV/s. Electrolyte: 50 mM KBr. Working electrode: GC.

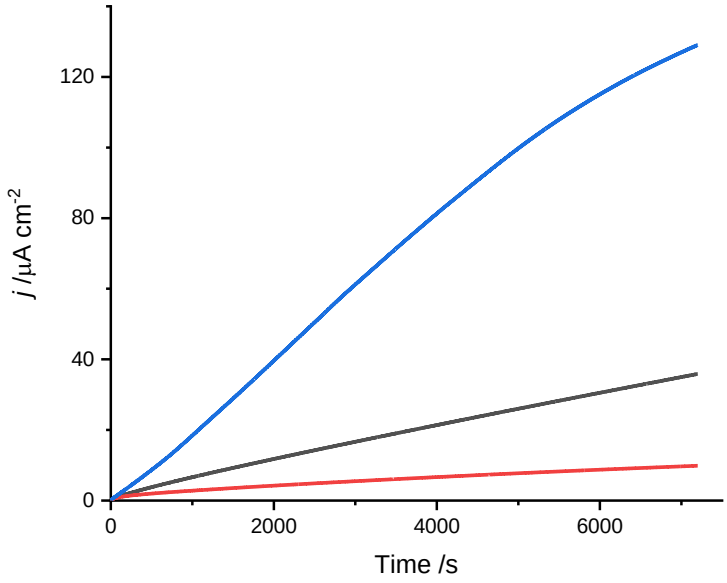

Figure S11. Charge passed during CPE for solutions of 0.1 M $NaNO_2$ (black), 0.5 mM $[Co(DIM)Br_2]^+$ (red) and 0.5 mM $[Co(DIM)Br_2]^+$ with 0.1 M $NaNO_2$ (blue). Carbon rod working electrode, initial pH = 7.2. Potential applied: -1.05 V *vs.* SCE.

Electrochemical Calculations

After the solution (0.5 mM $[Co(DIM)Br_2]^+$ + 100 mM $NaNO_2$, 15 mL, pH = 7.2) was electrolyzed under -1.05 V vs SCE for 2hr, the amount of NH_3 generated through CPE at -1.05 V vs SCE was quantified by the indophenol method[4] as 0.142 mmol.

(1) Faradaic efficiency calculation. Since ammonia quantification showed 0.142 mmol NH_3 was generated by the CPE experiment (after background subtraction), 0.85 mmol electrons (82 C) were used for NH_3 generation.

$$NO_2^- + 7H^+ + 6e^- \rightarrow NH_3 + 2H_2O$$

Since 93 C (background subtracted) electrons were consumed in total according to the total charge accumulation diagram, the Faraday efficiency can be calculated as:

(e^- used for NH_3 generation)/ (total e^- consumed) = 82/93 = 88 %.

(2) Turnover number (TON) calculation. Since total 7.5 μmol $[Co(DIM)Br_2]^+$ was used for electrocatalysis and 0.142 mmol NH_3 was generated during electrolysis, turnover number (TON) = 142/7.5 = 18.9 for the 2 h electrolysis.

(3) Rate constant (k) calculation from CV data. Similar to the literature precedent of rate constant calculation under pure kinetic condition,[7-8] the rate constant can be obtained by the following equations:

$$\text{(i)} \qquad i_p = 0.4463\ n_p^{3/2} F A C_p (F \nu D/RT)^{1/2}$$

$$\text{(ii)} \qquad i_c = n_c F A C_p (DkC_A)^{1/2}$$

In the electrocatalytic reduction of nitrite to ammonia, 6 electrons are consumed, $n_c = 6$. Since $[Co(DIM)(NO_2)_2]^+$ is reduced by two separate one-electron reductive processes, $n_p = 1$. By dividing equation (i) by (ii), equation (iii) can be obtained:

$$\text{(iii)} \qquad i_c = 13.45 \times i_p \nu^{-1/2} \times (RT/F)^{1/2} \times (kC_A)^{1/2}$$

In these equations,

i_p = maximum non-catalytic current

i_c = maximum catalytic current

n_p = number of electrons transferred in the non-catalytic event.

F = Faraday constant

A = area of the electrode = 0.09 cm^2

C_A = bulk concentration of the catalyst

n = scan rate

D = diffusion constant of catalyst

T = temperature

k = rate constant of catalytic reaction

Since the second reductive process at *ca.* -1.0 V vs SCE, Co^{II}-DIM/Co^{II}-DIM^-) overlaps with catalytic wave, this process cannot be observed directly. Based on the assumption that diffusion constant of $[Co(DIM)(NO_2)_2]^+$ is similar to that of the Co^{II}-DIM species, we applied equation (i) to analyze the first reversible wave ($E_{1/2}$ ~ -0.30 V vs SCE, Co(III)/(II)) to obtain data for further calculation to obtain value of $i_p\nu^{-1/2}$, which is equal to the slope of the i_p vs $\nu^{1/2}$ plot (slope = 3×10^{-5}, Figure S12). After $i_p\nu^{-1/2}$ is obtained from analysis of 1st reductive wave (Co(III)/(II)), k can be calculated according to equation (iii).

These calculations give TOF = 118 s^{-1}. Note that this value differs from that obtained from the CPE experiment described above because these values are obtained under slightly different conditions. Specifically, since the CPE determination was conducted under buffer-free conditions there is an increase in pH during the course of the electrolysis, whereas for the CV determination there is no pH change. It is also evident that there is loss of catalytic activity after longer time periods during the CPE experiment (Figure S11). Since the CPE experiment was conducted in order to characterize the nitrite reduction products, we did not attempt to optimize these conditions.

Note that no ammonia was detected for the CPE of $[Co(DIM)Br_2]^+$ in the absence of $NaNO_2$.

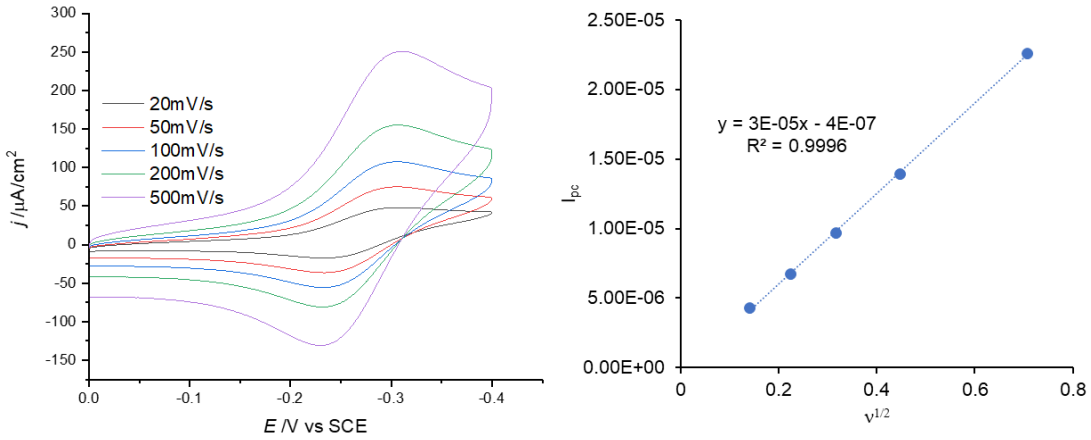

Figure S12. Cyclic voltammogram of 0.5 mM $[Co(DIM)Br_2]^+$ with 50 mM $NaNO_2$ at different scan rates (left). Plot of peak cathodic current i_p vs square root of scan rate $\nu^{1/2}$. In this plot, according to equation (i), $i_p\nu^{-1/2}$ is equal to the slope of plot, 3×10^{-5}. The data obtained from this Figure is applied to the rate constant calculation.

Variable Scan Experiments for Catalytic NO_2^- Reduction (Pure Kinetic Condition).

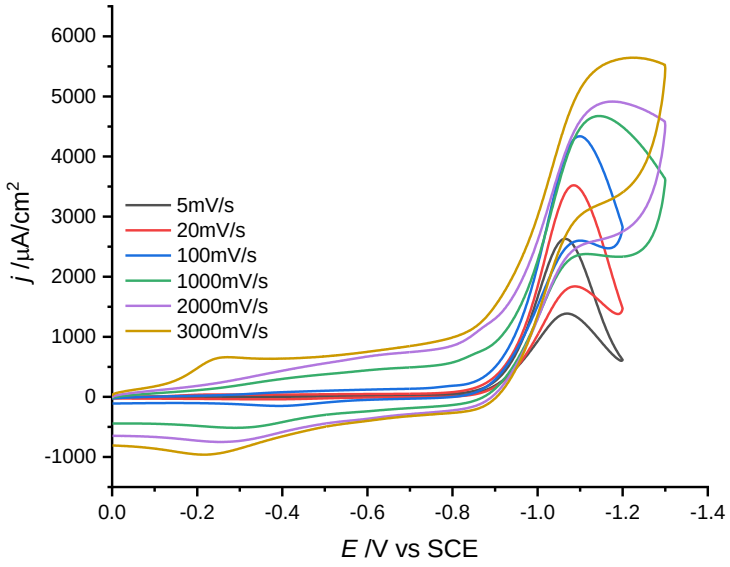

Figure S13. Cyclic voltammograms of 0.5 mM $[Co(DIM)Br_2]^+$ with 10 mM $NaNO_2$ at pH = 6.0 under different scan rates. Electrolyte: 100 mM Na_2SO_4. Working electrode: GC. Pure kinetic conditions (S-shaped CV) are achieved at ν = 3 V/s.

Cyclic Voltammogram of Catalytic NO_2^- Reduction Under Acidic pH

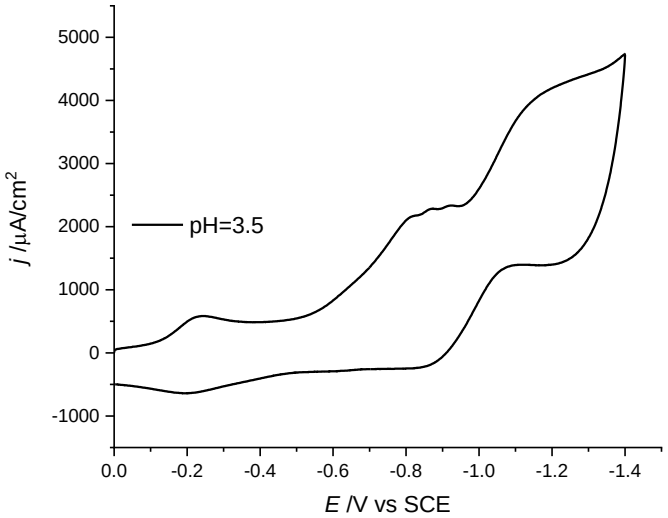

Figure S14. Cyclic voltammograms of 0.5 mM $[Co(DIM)Br_2]^+$ with 10 mM $NaNO_2$ at pH = 3.5. Electrolyte: 100 mM Na_2SO_4. Working electrode: GC. Scan rate = 3 V/s.

Calculation of Activation Parameters

To calculate activation parameters of the reaction, the cyclic voltammograms of electrocatalytic NO_2^- reduction were recorded at different temperatures. According to the CVs, the rate constant for each temperature, k, is calculated according to the equation: $i_c = n_c FAC_p(DkC_A)^{1/2}$.[9] The plot of ln($k$/T) vs. (1/T) fit to the equation: y = -3678.9x + 17.13. $\Delta H^{\ddagger}$ and $\Delta S^{\ddagger}$ are calculated according to the Eyring equation: $\ln(k/T) = (-\Delta H^{\ddagger}/R)\times(1/T) + \ln(\kappa k_B/h) + \Delta S^{\ddagger}/R$.

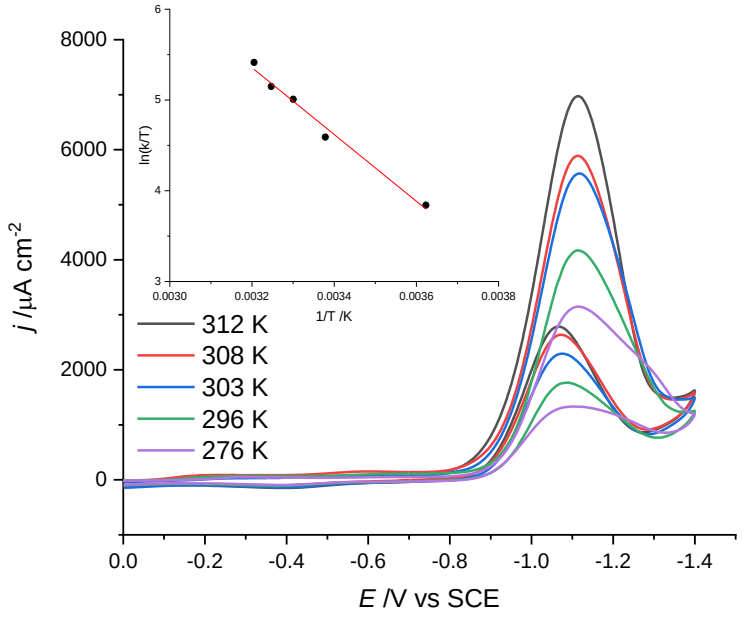

Figure S15. Cyclic voltammograms of 0.5 mM $[Co(DIM)Br_2]^+$ with 20 mM $NaNO_2$ at variable temperatures, pH = 6.0. Electrolyte: 100 mM Na_2SO_4. Working electrode: GC. Inset: plot of ln(k/T) vs 1/T for activation parameter calculation.

CVs for Kinetic Isotope Effect (KIE) Value Calculation

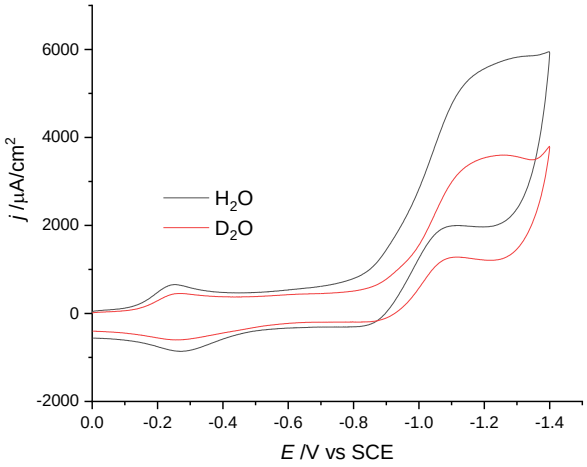

Figure S16. CVs of $[Co(DIM)Br_2]^+$ recorded in D_2O (red) and H_2O (black). Conditions: 0.5 mM $[Co(DIM)Br_2]^+$ with 10 mM $NaNO_2$, pH = 6.0. GC working electrode, 100 mM Na_2SO_4, scan rate: 3 V/s for H_2O experiment while 2.5 V/s for D_2O experiment. KIE value was calculated based on peak current ratio at -1.2 V vs. SCE, KIE = $k_H/k_D = (i_{p,H}/i_{p,D})^2$.[10]

^{1}H NMR spectra of $[Co(DIM)Br_2]^+$ in CD_3OD

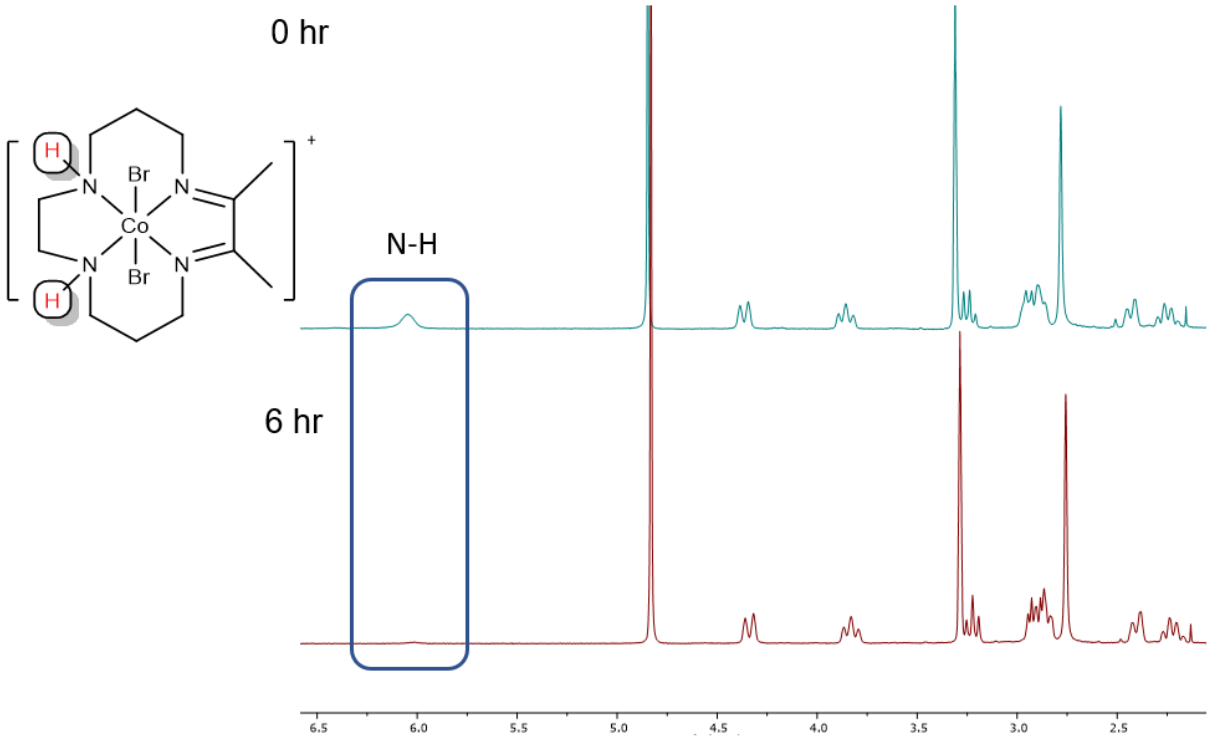

Figure S17. ^{1}H NMR spectra of $[Co(DIM)Br_2]^+$ in CD_3OD. Resonance for amine protons (δ *ca.* 6.0 ppm) are circled. In CD_3OD, this peak disappears over the course of several hours due to exchange with deuterium.

Macrocycle Properties

The catalytic activity of related macrocyclic complexes, $[Co(cyclam)Cl_2]^+$ [11] and $[Co(TIM)Br_2]^+$ (TIM = 2,3,9,10-tetramethyl-1,4,8,11- tetraazacyclotetradeca-1,3,8,10-tetraene)[1] toward NO_2^- reduction were characterized to investigate the ligand effect. According to CVs summarized in Figure S18, $[Co(DIM)Br_2]^+$ exhibits superior catalytic activity as compared to $[Co(cyclam)Cl_2]^+$ (redox inactive ligand) and $[Co(TIM)Br_2]^+$ (no N-H hydrogen available for intramolecular H-bonding), which is consistent with the hypothesis that both redox noninnocence and N-H hydrogens are essential to the catalytic activity.

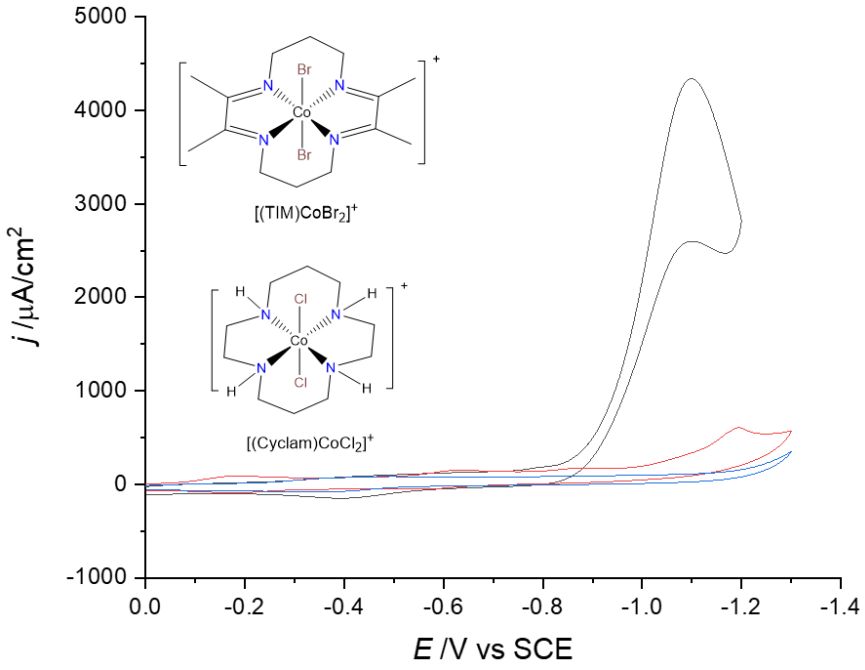

Figure S18. Cyclic voltammograms of 0.5 mM $[Co(DIM)Br_2]^+$ (black), $[Co(TIM)Br_2]^+$ (red) and $[Co(cyclam)Cl_2]^+$ (blue) with 10 mM $NaNO_2$. GC electrode, 100 mM Na_2SO_4, scan rate = 100 mV/s, pH = 6.0. Inset: structure of $[Co(TIM)Br_2]^+$ and $[Co(cyclam)Cl_2]^+$.

Computational Methods

All structures were optimized with the B3LYP[12-15] functional including Grimme's D2 dispersion correction[16] (B3LYP+D2), unless noted otherwise. These optimizations were performed using the implicit SMD[17] model to account for solvent effects using either water or acetonitrile depending on what experimental results were being compared to. Frequencies were calculated for all optimized structures using the harmonic oscillator approximation to verify that the structures were true minima with no imaginary frequencies. The results of these frequency calculations were also used to calculate zero-point energy and entropic corrections to the free energy at 298.15 K and 1.0 atm using standard statistical mechanical conventions. Additionally, wavefunction stability tests were performed on all complexes to verify the nature of the electronic state, and only complexes with stable wavefunctions were reported.

A smaller basis set (BS-I) was used for the geometry optimizations and the frequency calculations. The electronic energies were then determined from single point energy calculations performed on these geometries with a larger basis set (BS-II) that also incorporated diffuse functions. Both BS-I and BS-II employed an SDD pseudopotential (ECP10MDF) and accompanying basis set for Co.[18-19] Br was also modeled with an SDD pseudopotential (ECP10MDF) and associated cc-pVTZ-PP basis set for BS-I, while the larger aug-cc-pVTZ-PP basis set was used for BS-II.[20] All other atoms used 6-31G* for BS-I[21-22] and 6-311+G** for BS-II.[23-24] An ultrafine grid was used for all calculations. The final solvated free energy (G_{sol}) was then adjusted[25] to have the standard state concentration of 1 M or 55.5 M for water, a correction of -1.9 and -4.3 kcal/mol, respectively. All DFT calculations were performed with the Gaussian 16 software package Revision A.03.[26]

Calculated reduction potentials (E^0) were determined relative to the normal hydrogen electrode (NHE) through equation S1:

$$E°(\text{eV}) = -\frac{\Delta G_{sol}}{nF} - 4.28 \qquad \text{(Eq. S1)}$$

Here, ΔG_{sol} is the change in solvated free energy upon reduction, n is the number of electrons transferred, in our case this is always one, and F is Faraday's constant. The calculated potentials are referenced to NHE by subtracting the absolute reduction potential of NHE, 4.28 V.[27] This value of NHE is determined by the aqueous solvation free energy of the proton, 265.9 kcal/mol, and this solvation energy was also used when calculating pK_as and/or the solvated free energy of H^+. Note that much work has been done on determining the absolute value of NHE, and not all estimates agree,[27-32] and hence our calculated values may be subject to a modest systematic error. Finally, the calculated values vs. NHE are all reported relative to SCE (0.2412 vs. NHE)[33].

MECPs were optimized using a freely available code that interfaces with Gaussian 09 (here Gaussian Revision D.01 was used) from Harvey and co-workers.[34] These geometries were used to calculate the single point energies reported in the text, using Gaussian 16. The MECP optimizations and single point energy calculations were all performed at the same level of theory described above.

O-bound Nitrite Reduction Mechanism

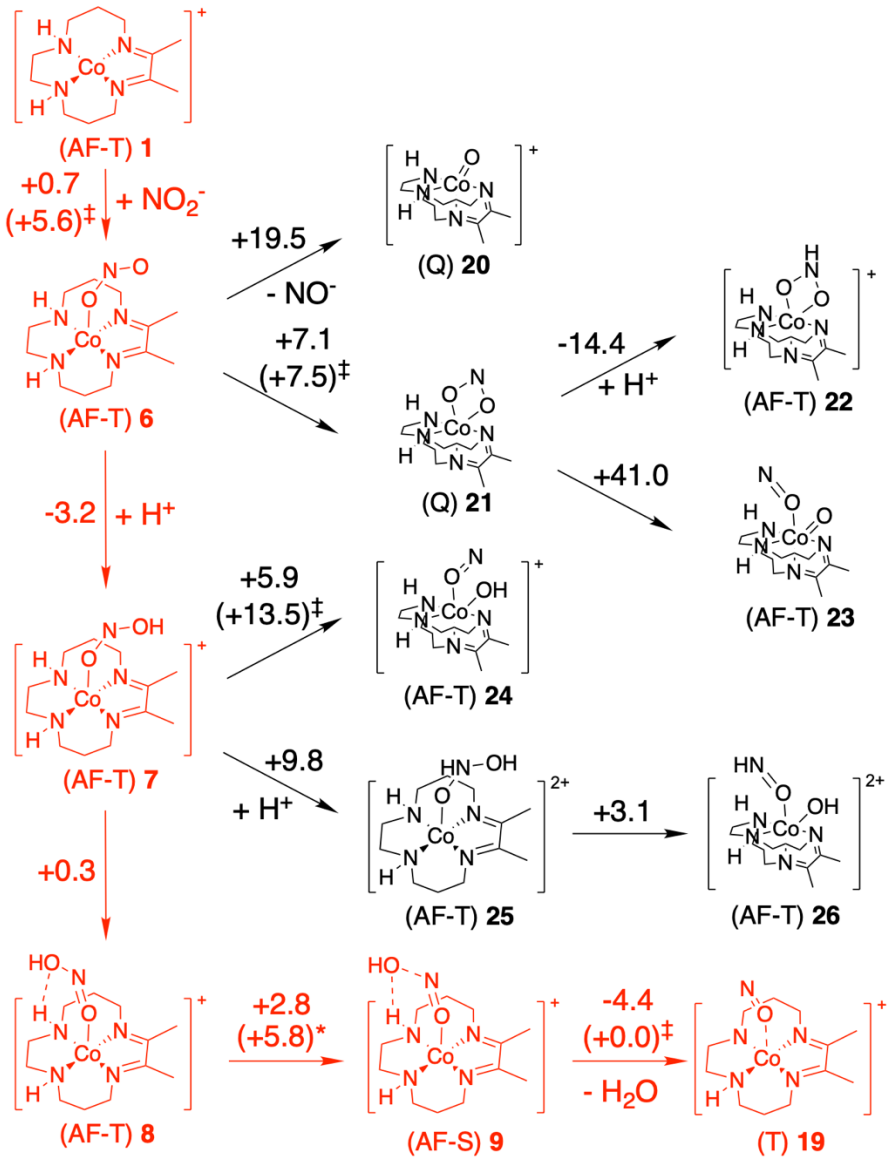

Figure S19. Oxygen bound nitrite reduction mechanisms examined with DFT with energy corrections at pH=6 (ΔG is reported in kcal/mol).

Several plausible O-bound mechanisms were investigated. The most favored mechanism in the figure S19 is also an amino-proton-assisted mechanism (red) with the activation barrier of 6.1 kcal/mol. However, as shown in figure 5, shifting the protonated nitro ligand to N-bound (the **10-**

4 transition state energy relative to complex **8**) has 2.5 kcal/mol lower barrier than the O-bound amino-proton-assisted mechanism (the **8-9** MECP energy relative to complex **8**).

Electronic Structure for AF-T and AF-S of $[Co(DIM)(HNO_2)]^+$

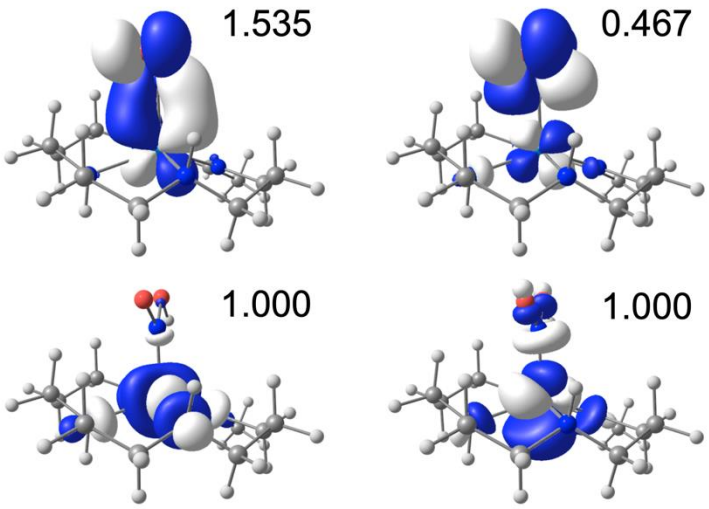

Figure S20. $[Co(DIM)(HNO_2)]^+$ AF-triplet natural orbitals. The occupation numbers of each NO are indicated.

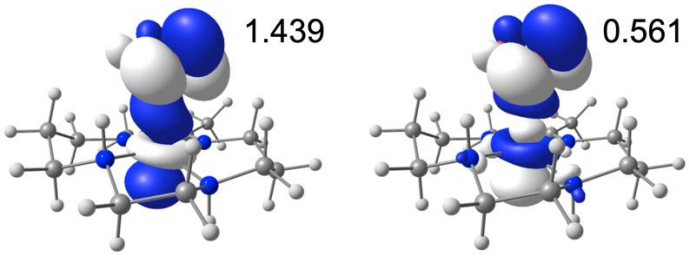

Figure S21. $[Co(DIM)(HNO_2)]^+$ AF-singlet natural orbitals. The occupation numbers of each NO are indicated.

The degree of pyramidalization of the HNO_2 group is indicated by the measured out-of-plane angle of the nitrogen atom (this can also be referred to as an improper dihedral). This is 6.1° for AF-

triplet geometry and 37.3° for AF-singlet geometry. The AF-coupled orbitals are Co-N σ and σ* in singlet while π and π* in triplet preventing its HNO_2 geometry from bending to tetrahedral.

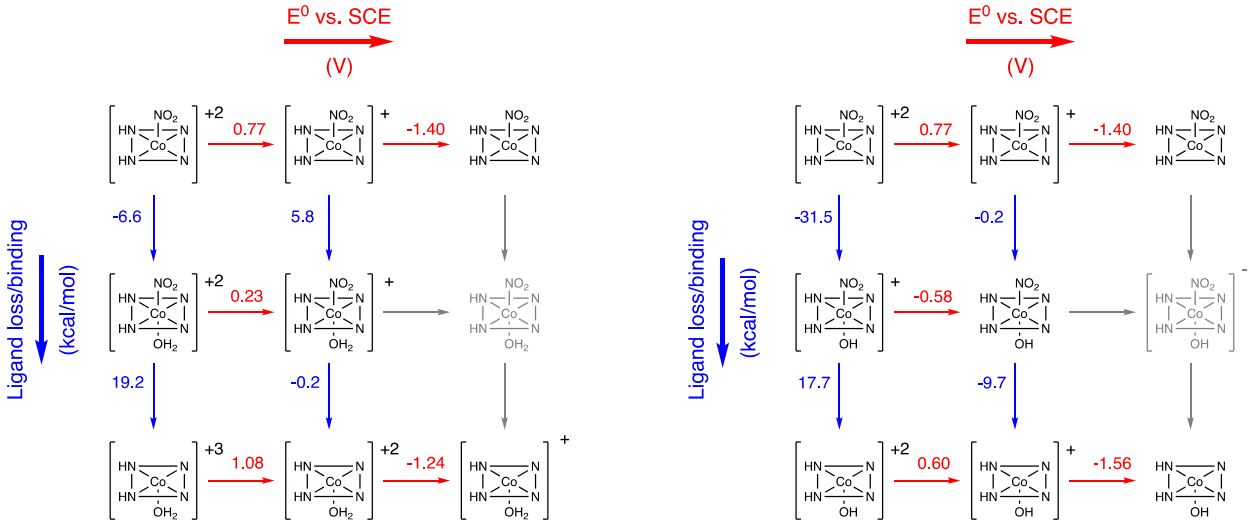

Figure S22. Additional square schemes related to speciation and electrochemistry.

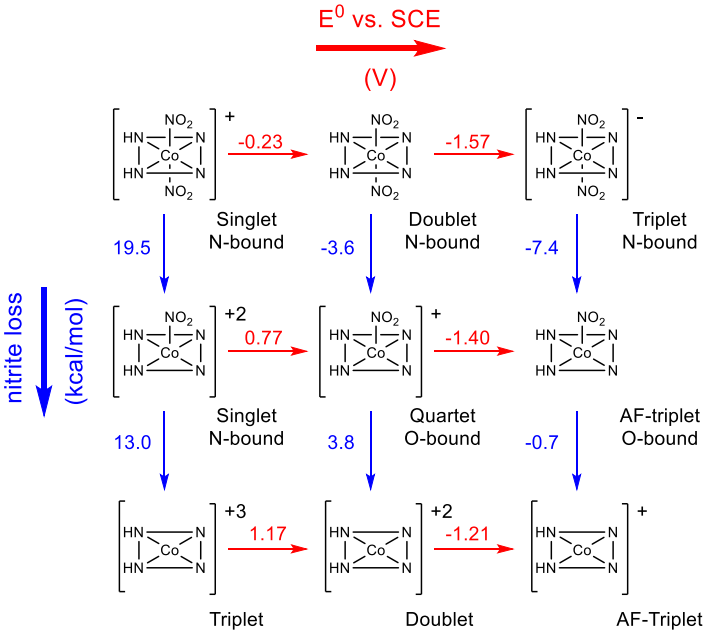

Figure S23. More detailed version of Scheme 3. The lowest energy spin state and nitrite-binding mode (when applicable) are indicated below each structure.

Table S1. Electronic energies (E), zero-point energies (ZPE), entropic corrections to free energies (−TS), enthalpies (H), and solvated Gibbs free energies (G_{sol}) calculated with DFT. Solvated free energies not adjusted for concentration are listed as G′. All optimizations were done with the SMD correction for solvent (water unless specified otherwise), hence E contains the solvation effects. The temperature (T) was set to 298.15 K, and the pressure to 1 atm. All values are reported in kcal/mol. The concentration of all species is considered to be 1 M with the exception of water, which is treated as 55.5 M.

Compound	E	ZPE	-TΔS	H	G_{sol}	G'
Nitrite	-128847.37	4.91	-17.30	-128775.90	-128855.44	-128857.33
Water	-47986.89	13.15	-13.87	-47938.86	-47980.96	-47985.24
Hydroxide	-47677.25	5.17	-12.28	-47611.90	-47680.39	-47682.28
NO^-	-81613.89	2.06	-14.99	-81562.87	-81622.84	-81624.74
$[Co\text{-}DIM]^{3+}$ (III) singlet	-524879.88	233.00	-37.01	-524518.43	-524671.34	-524673.24
$[Co\text{-}DIM]^{3+}$ (III) triplet	-524893.92	232.80	-38.95	-524532.12	-524686.99	-524688.89
$[Co\text{-}DIM]^{3+}$ (III) quintet	-524881.00	230.76	-40.14	-524519.56	-524676.83	-524678.72
$[Co\text{-}DIM]^{2+}$ (II) quartet	-525021.30	230.80	-40.97	-524658.94	-524817.69	-524819.58
$[Co\text{-}DIM]^{2+}$ (II) doublet	-525024.36	232.57	-39.73	-524661.55	-524818.27	-524820.17
$[Co\text{-}DIM]^{+}$ (I) singlet	-525098.87	230.91	-38.74	-524734.80	-524893.35	-524895.24
$[Co\text{-}DIM]^{+}$ (I) triplet	-525099.46	231.15	-38.99	-524735.31	-524894.10	-524896.00
$[Co\text{-}DIM]^{+}$ (I) AF-triplet	-525097.66	229.75	-40.48	-524734.12	-524894.72	-524896.61
$[Co\text{-}DIM]^{+}$ (I) quintet	-525094.30	229.46	-40.30	-524730.65	-524891.50	-524893.39
$[Co\text{-}DIM(H_2O)]^{3+}$ (III) singlet	-572886.18	250.70	-40.62	-572482.13	-572661.85	-572663.75
$[Co\text{-}DIM(H_2O)]^{3+}$ (III) triplet	-572891.38	249.94	-41.28	-572487.28	-572668.32	-572670.22
$[Co\text{-}DIM(H_2O)]^{3+}$ (III) quintet	-572873.19	248.01	-42.48	-572470.18	-572652.86	-572654.76
$[Co\text{-}DIM(H_2O)]^{2+}$ (II) doublet	-573017.96	248.67	-43.02	-572612.61	-572797.43	-572799.33
$[Co\text{-}DIM(H_2O)]^{2+}$ (II) quartet	-573017.39	247.88	-42.46	-572612.61	-572797.09	-572798.99
$[Co\text{-}DIM(H_2O)]^{+}$ (I) triplet	-573090.69	246.58	-43.08	-572684.05	-572872.12	-572874.02
$[Co\text{-}DIM(H_2O)]^{+}$ (I) AF-singlet	-573090.95	247.03	-41.81	-572684.23	-572870.82	-572872.72
$[Co\text{-}DIM(H_2O)]^{+}$ (I) AF-triplet	-573090.40	245.55	-43.64	-572684.45	-572873.13	-572875.03
$[Co\text{-}DIM(H_2O)]^{+}$ (I) quintet	-573085.51	245.04	-43.71	-572679.66	-572868.81	-572870.70
$[Co\text{-}DIM(OH)]^{2+}$ (III) singlet	-572609.53	241.64	-40.51	-572215.85	-572394.16	-572396.06
$[Co\text{-}DIM(OH)]^{2+}$ (III) triplet	-572609.49	242.04	-40.66	-572215.91	-572394.07	-572395.97
$[Co\text{-}DIM(OH)]^{2+}$ (III) quintet	-572602.08	239.87	-42.74	-572210.31	-572390.24	-572392.14
$[Co\text{-}DIM(OH)]^{+}$ (II) quartet	-572722.29	238.64	-43.79	-572326.46	-572512.36	-572514.26
$[Co\text{-}DIM(OH)]^{+}$ (II) doublet	-572714.17	240.11	-41.79	-572315.65	-572501.29	-572503.19
[Co-DIM(OH)] (I) AF-singlet	-572783.60	238.64	-40.80	-572382.74	-572571.25	-572573.14

[Co-DIM(OH)] (I) triplet	-572780.68	237.83	-42.16	-572379.21	-572570.26	-572572.15
[Co-DIM(OH)] (I) AF-triplet	-572789.63	237.14	-43.20	-572391.54	-572580.60	-572582.49
[Co-DIM(OH)] (I) quintet	-572784.12	236.59	-43.70	-572386.26	-572576.02	-572577.92
$[Co\text{-}DIM(NO_2)_2]^+$ (III) singlet (N-bound)	-782650.47	249.55	-46.04	-782179.41	-782430.30	-782432.19
$[Co\text{-}DIM(NO_2)_2]^+$ (III) triplet (N-bound)	-782597.12	247.21	-47.04	-782128.66	-782380.11	-782382.00
$[Co\text{-}DIM(NO_2)_2]$ (II) doublet (N-bound)	-782729.57	247.56	-46.91	-782256.39	-782512.09	-782513.99
$[Co\text{-}DIM(NO_2)_2]$ (II) doublet (N-bound)	-782742.27	245.40	-50.61	-782265.03	-782529.36	-782531.25
$[Co\text{-}DIM(NO_2)_2]$ (II) quartet (N-bound)	-782737.10	244.01	-51.16	-782261.36	-782525.90	-782527.79
$[Co\text{-}DIM(NO_2)_2]^-$ (I) AF-singlet (N-bound)	-782807.51	243.48	-50.55	-782326.87	-782596.30	-782598.20
$[Co\text{-}DIM(NO_2)_2]^-$ (I) triplet (N-bound)	-782808.49	243.61	-50.68	-782327.93	-782597.42	-782599.32
$[Co\text{-}DIM(NO_2)_2]^-$ (I) AF-triplet (N-bound)	-782804.56	242.24	-51.13	-782325.48	-782594.97	-782596.86
$[Co\text{-}DIM(NO_2)_2]^-$ (I) quintet (N-bound)	-782801.19	242.15	-51.74	-782322.08	-782592.27	-782594.16
$[Co\text{-}DIM(NO_2)]^{2+}$ (III) singlet (N-bound)	-653769.62	241.42	-42.10	-653353.63	-653555.41	-653557.31
$[Co\text{-}DIM(NO_2)]^{2+}$ (III) triplet (N-bound)	-653761.54	239.69	-45.20	-653344.72	-653551.52	-653553.42
$[Co\text{-}DIM(NO_2)]^+$ (II) doublet (N-bound)	-653885.77	239.26	-44.83	-653466.11	-653675.81	-653677.71
$[Co\text{-}DIM(NO_2)]^+$ (II) quartet (N-bound)	-653881.93	237.93	-46.26	-653462.63	-653674.31	-653676.20
$[Co\text{-}DIM(NO_2)]$ (I) AF-singlet (N-bound)	-653957.69	237.88	-43.79	-653536.16	-653748.10	-653749.99
$[Co\text{-}DIM(NO_2)]$ (I) triplet (N-bound)	-653955.54	237.51	-44.74	-653533.71	-653747.16	-653749.05
$[Co\text{-}DIM(NO_2)]$ (I) AF-triplet (N-bound)	-653955.92	236.60	-45.30	-653535.10	-653748.70	-653750.60
$[Co\text{-}DIM(NO_2)]$ (I) quintet (N-bound)	-653950.05	236.02	-46.38	-653529.00	-653744.31	-653746.20
$[Co\text{-}DIM(NO_2)(H_2O))]^{2+}$ (III) Singlet (N-bound)	-701775.09	259.87	-43.47	-701315.90	-701542.97	-701544.87
$[Co\text{-}DIM(NO_2)(H_2O)]^{2+}$ (III) triplet (N-bound)	-701757.06	256.92	-47.05	-701297.68	-701530.45	-701532.35
$[Co\text{-}DIM(NO_2)(H_2O)]^+$ (II) doublet (N-bound)	-701876.46	254.98	-48.53	-701413.96	-701652.64	-701654.54
$[Co\text{-}DIM(NO_2)(H_2O)]^+$ (II) quartet (N-bound)	-701872.12	253.64	-49.24	-701411.10	-701650.15	-701652.04
$[Co\text{-}DIM(NO_2)(OH)]^+$ (III) singlet (N-bound)	-701488.24	249.73	-44.81	-701038.45	-701267.27	-701269.17
$[Co\text{-}DIM(NO_2)(OH)]^+$ (III) triplet (N-bound)	-701464.18	247.77	-45.95	-701016.40	-701245.87	-701247.77
$[Co\text{-}DIM(NO_2)(OH)]$ (II) doublet (N-bound, ligand reduced)	-701564.36	247.87	-44.55	-701112.23	-701344.95	-701346.85
$[Co\text{-}DIM(NO_2)(OH)]$ (II) doublet (N-bound, metal reduced)	-701569.15	246.38	-47.13	-701112.00	-701352.87	-701354.77
$[Co\text{-}DIM(NO_2)_2]^+$ (III) singlet (O-bound)	-782641.83	247.57	-48.29	-782172.95	-782425.26	-782427.16
$[Co\text{-}DIM(NO_2)_2]^+$ (III) triplet (O-bound)	-782624.46	245.56	-50.14	-782154.93	-782411.10	-782413.00
$[Co\text{-}DIM(NO_2)_2]$ (II) doublet (O-bound)	-782738.15	244.42	-52.14	-782263.40	-782527.35	-782529.25
$[Co\text{-}DIM(NO_2)_2]$ (II) quartet (O-bound)	-782734.51	242.46	-54.06	-782261.77	-782527.14	-782529.04
$[Co\text{-}DIM(NO_2)_2]^-$ (I) AF-singlet (O-bound)	-782803.67	242.69	-52.50	-782322.61	-782594.69	-782596.59

[Co-DIM(NO_2)$_2$]$^-$ (I) triplet (O-bound)	-782805.75	242.54	-52.60	-782327.81	-782597.13	-782599.03
[Co-DIM(NO_2)$_2$]$^-$ (I) AF-triplet (O-bound)	-782801.15	241.15	-51.10	-782323.19	-782592.68	-782594.57
[Co-DIM(NO_2)$_2$]$^-$ (I) quintet (O-bound)	-782799.18	240.94	-55.92	-782320.62	-782595.04	-782596.93
[Co-DIM(NO_2)]$^{2+}$ (III) singlet (O-bound)	-653763.85	240.44	-43.46	-653349.33	-653551.73	-653553.63
[Co-DIM(NO_2)]$^{2+}$ (III) triplet (O-bound)	-653762.22	239.20	-44.86	-653347.38	-653552.36	-653554.26
[Co-DIM(NO_2)]$^+$ (II) doublet (O-bound)	-653882.90	238.55	-45.44	-653464.91	-653674.01	-653675.91
[Co-DIM(NO_2)]$^+$ (II) quartet (O-bound)	-653884.33	237.39	-46.76	-653467.60	-653677.49	-653679.39
[Co-DIM(NO_2)] (I) AF-singlet (O-bound)	-653954.32	237.15	-44.57	-653534.25	-653745.94	-653747.84
[Co-DIM(NO_2)] (I) triplet (O-bound)	-653953.42	236.90	-45.38	-653533.08	-653746.05	-653747.95
[Co-DIM(NO_2)] (I) AF-triplet (O-bound)	-653955.67	236.11	-46.01	-653536.85	-653749.43	-653751.33
[Co-DIM(NO_2)] (I) quintet (O-bound)	-653949.65	235.33	-47.79	-653531.08	-653745.69	-653747.59
[Co-DIM(NO_2)(H_2O))]$^{2+}$ (III) singlet (O-bound)	-701770.87	258.74	-44.16	-701313.30	-701540.24	-701542.14
[Co-DIM(NO_2)(H_2O)]$^{2+}$ (III) triplet (O-bound)	-701756.39	256.76	-46.31	-701298.37	-701529.29	-701531.19
[Co-DIM(NO_2)(H_2O)]$^+$ (II) doublet (O-bound)	-701874.28	254.45	-48.82	-701413.06	-701651.13	-701653.02
[Co-DIM(NO_2)(H_2O)]$^+$ (II) quartet (O-bound)	-701871.45	253.12	-49.93	-701410.73	-701650.39	-701652.29
[Co-DIM(NO_2)(OH)]$^+$ (III) singlet (O-bound)	-701484.02	248.98	-44.67	-701035.59	-701263.48	-701265.38
[Co-DIM(NO_2)(OH)]$^+$ (III) triplet (O-bound)	-701461.84	246.97	-46.30	-701015.02	-701244.43	-701246.33
[Co-DIM(NO_2)(OH)] (II) doublet (O-bound, ligand reduced)	-701558.63	247.10	-45.03	-701108.13	-701340.25	-701342.15
[Co-DIM(NO_2)(OH)] (II) doublet (O-bound, metal reduced)	-701567.08	245.99	-48.32	-701109.44	-701352.14	-701354.03
[Co-DIM(NO_2)(OH)] (II) quartet (O-bound)	-701570.17	244.09	-49.67	-701116.50	-701358.05	-701359.95
Fig.9 1-2 TS AF-singlet	-653951.54	236.92	-44.42	-653528.66	-653743.44	-653745.34
Fig.9 1-2 TS triplet	-653952.17	236.92	-45.12	-653529.10	-653744.78	-653746.68
Fig.9 1-6 TS triplet	-653951.78	236.77	-45.13	-653529.49	-653744.56	-653746.45
Fig.9 1-6 TS quintet	-653946.67	235.03	-46.51	-653525.09	-653742.07	-653743.97
Fig.9 3 AF-singlet	-654248.45	245.48	-44.52	-653817.99	-654031.61	-654033.50
Fig.9 3 triplet	-654245.83	245.42	-45.38	-653814.46	-654029.82	-654031.71
Fig.9 3 AF-triplet	-654249.33	244.22	-46.05	-653819.95	-654034.87	-654036.77
Fig.9 3 AF-quintet	-654244.05	244.09	-46.81	-653812.74	-654030.34	-654032.24
Fig.10 3-13 TS singlet	-654228.93	246.35	-42.43	-653801.87	-654009.96	-654011.85
Fig.10 4 AF-triplet	-654247.67	243.79	-46.31	-653819.07	-654033.81	-654035.71
Fig.10 4-5 TS singlet	-654227.81	245.33	-43.18	-653800.84	-654010.33	-654012.22
Fig.10 4-5 MECP AF-singlet	-654243.58	243.70	-44.31	-653815.10	-654028.32	-654030.21
Fig.10 4-5 MECP AF-triplet	-654243.20	243.30	-47.58	-653814.76	-654030.88	-654032.77
Fig.9 4-10 TS AF-singlet	-654236.15	244.57	-44.02	-653809.27	-654019.97	-654021.86
Fig.9 4-10 TS AF-triplet	-654242.67	243.43	-44.82	-653816.78	-654028.43	-654030.32
Fig.9 4-10 TS quintet	-654233.16	243.08	-46.38	-653806.25	-654020.24	-654022.14

Fig.10 5 AF-singlet	-654248.23	244.97	-44.41	-653818.51	-654031.74	-654033.64
Fig.9 5 triplet	-654243.75	244.67	-45.71	-653814.02	-654028.64	-654030.53
Fig.10 5-11 TS AF-singlet	-654247.15	246.91	-45.10	-653816.76	-654035.50	-654037.40
Fig.10 5-11 TS triplet	-654230.49	240.83	-45.59	-653797.01	-654019.09	-654020.99
Fig. S19 6-21 TS quintet	-653948.09	235.61	-45.23	-653531.24	-653741.95	-653743.84
Fig.9 7 AF-singlet	-654243.93	244.89	-45.22	-653815.42	-654028.17	-654030.06
Fig.9 7 AF-triplet	-654245.38	244.45	-46.30	-653817.84	-654031.01	-654032.91
Fig.9 7 quintet	-654243.44	244.45	-46.44	-653815.55	-654029.19	-654031.08
Fig.S19 7-24 TS singlet	-654194.36	245.46	-41.81	-653768.50	-653975.77	-653977.66
Fig.S19 7-24 TS triplet	-654232.67	244.41	-45.05	-653805.89	-654017.55	-654019.45
Fig.9 8 AF-triplet	-654245.42	244.46	-45.99	-653817.89	-654030.74	-654032.64
Fig.9 8 quintet	-654243.48	244.41	-46.69	-653815.57	-654029.47	-654031.37
Fig.9 8-9 MECP AF-singlet	-654241.41	244.43	-43.52	-653814.75	-654024.92	-654026.82
Fig.9 8-9 MECP AF-triplet	-654241.26	243.90	-45.52	-653815.04	-654027.04	-654028.94
Fig.9 8-10 TS AF-singlet	-654234.01	244.91	-43.22	-653808.30	-654016.87	-654018.76
Fig.9 8-10 TS AF-triplet	-654243.18	243.74	-45.14	-653818.34	-654028.75	-654030.65
Fig.9 9 AF-singlet	-654244.37	245.20	-44.74	-653816.37	-654027.96	-654029.85
Fig.S19 9-19 TS AF-singlet	-654238.53	240.36	-45.81	-653810.52	-654027.72	-654029.62
Fig.9 10 singlet	-654236.64	246.46	-42.29	-653810.46	-654017.24	-654019.14
Fig.9 10 AF-triplet	-654243.53	243.63	-46.70	-653818.51	-654030.21	-654032.11
Fig.10 11 AF-singlet	-654249.11	242.52	-45.94	-653817.56	-654035.93	-654037.83
Fig.10 11 triplet	-654240.98	242.43	-46.85	-653808.91	-654028.69	-654030.58
Fig.10 12 AF-singlet	-606254.26	227.54	-42.21	-605868.60	-606054.09	-606055.99
Fig.10 12 triplet	-606247.86	227.14	-43.47	-605862.01	-606049.18	-606051.08
Fig.10 12 quintet	-606238.32	226.13	-44.71	-605851.78	-606041.64	-606043.53
Fig.10 13 AF-singlet	-654248.00	245.28	-44.57	-653817.62	-654031.30	-654033.20
Fig.10 13-14 TS AF-singlet	-654240.03	244.98	-42.83	-653809.47	-654022.42	-654024.32
Fig.10 13-14 TS triplet	-654231.62	244.76	-43.83	-653802.34	-654015.13	-654017.03
Fig.10 13-17 TS AF-singlet	-654239.33	244.65	-43.76	-653811.08	-654022.75	-654024.64
Fig.10 13-17 TS triplet	-654252.74	242.81	-46.49	-653825.38	-654039.91	-654041.81
Fig.10 14 AF-singlet	-654252.19	246.10	-43.21	-653823.90	-654033.78	-654035.68
Fig.10 14 triplet	-654243.12	245.57	-44.34	-653814.76	-654026.24	-654028.14
Fig.10 15 AF-singlet	-654556.92	256.41	-42.53	-654119.27	-654327.71	-654329.60
Fig.10 15 triplet	-654547.37	255.70	-44.60	-654109.54	-654320.59	-654322.49
Fig.10 15-16 TS AF-singlet	-654503.70	251.55	-42.54	-654070.77	-654279.33	-654281.23
Fig.10 15-16 TS AF-triplet	-654500.73	249.97	-44.71	-654067.79	-654279.50	-654281.40
Fig.10 16 AF-singlet	-654556.93	252.95	-46.32	-654116.23	-654333.55	-654335.45
Fig.10 16 triplet	-654547.76	252.29	-48.10	-654107.00	-654326.49	-654328.38
Fig.10 17 singlet	-654253.77	247.08	-42.38	-653824.68	-654033.76	-654035.65
Fig.10 17 triplet	-654253.15	247.07	-42.52	-653824.13	-654033.26	-654035.16
Fig.10 18 AF-singlet	-606566.01	237.30	-42.41	-606170.69	-606356.24	-606358.14
Fig.10 18 triplet	-606556.89	237.09	-43.50	-606161.42	-606348.25	-606350.15
Fig.10 18 AF-triplet	-606557.81	235.31	-45.17	-606162.33	-606352.03	-606353.93

Fig.10 18 quintet	-606557.49	235.24	-45.47	-606162.03	-606352.05	-606353.95
Fig.S19 19 singlet	-606220.80	226.93	-42.55	-605835.15	-606021.51	-606023.41
Fig.S19 19 triplet	-606247.15	226.35	-46.24	-605861.03	-606051.39	-606053.29
Fig.S19 19 quintet	-606236.20	226.34	-44.80	-605849.01	-606039.33	-606041.23
Fig.S19 20 AF-singlet	-572291.32	233.22	-41.34	-571904.65	-572085.12	-572087.02
Fig.S19 20 triplet	-572298.52	234.10	-40.09	-571915.03	-572090.65	-572092.54
Fig.S19 20 quintet	-572311.18	233.10	-42.31	-571928.55	-572106.02	-572107.91
Fig. S19 21 quintet	-653947.90	235.75	-46.43	-653530.65	-653742.34	-653744.24
Fig. S19 22 AF-triplet	-654243.39	245.08	-45.20	-653817.82	-654027.50	-654029.40
Fig. S19 22 quintet	-654241.92	244.73	-46.28	-653816.24	-654027.25	-654029.15
Fig.S19 23 AF-singlet	-653905.45	238.31	-42.56	-653481.33	-653694.33	-653696.22
Fig.S19 23 AF-triplet	-653911.14	238.01	-43.80	-653488.06	-653701.38	-653703.27
Fig.S19 24 singlet	-654238.44	246.75	-42.26	-653809.45	-654018.64	-654020.54
Fig.S19 24 triplet	-654243.37	246.55	-43.70	-653814.58	-654025.12	-654027.01
Fig.S19 25 singlet	-654514.66	256.07	-42.24	-654078.22	-654285.63	-654287.53
Fig.S19 25 AF-triplet	-654523.35	253.53	-46.07	-654088.39	-654299.63	-654301.53
Fig.S19 25 quintet	-654522.53	253.67	-46.28	-654087.37	-654298.95	-654300.85
Fig.S19 26 singlet	-654524.82	255.08	-42.05	-654089.73	-654296.54	-654298.43
Fig.S19 26 triplet	-654503.96	253.79	-43.88	-654068.42	-654278.27	-654280.17

Crystallographic Data Collection

$[Co^{III}(DIM)(NO_2)_2]BPh_4$

Data collection

A preliminary set of cell constants was calculated from reflections harvested from three sets of 12 frames. These initial sets of frames were oriented such that orthogonal wedges of reciprocal space were surveyed. This produced initial orientation matrices determined from 1281 reflections. The data collection was carried out using Mo Kα radiation (graphite monochromator) with a frame time of 90 seconds and a detector distance of 4.0 cm. A randomly oriented region of reciprocal space was surveyed to achieve complete data with a redundancy of 4. Sections of frames were collected with 0.50º steps in ω and ϕ scans. Data to a resolution of 0.80 Å were considered in the reduction. Final cell constants were calculated from the xyz centroids of 9907 strong reflections from the actual data collection after integration (SAINT).[35] The intensity data were corrected for absorption (SADABS).[36] Please refer to Table S2 for additional crystal and refinement information.

Structure solution and refinement

The space group P 1 21/n 1 was determined based on intensity statistics and systematic absences. The structure was solved using Superflip[37] and refined (full-matrix-least squares) using the Oxford University Crystals for Windows system.[38] The charge-flipping solution provided most non-hydrogen atoms from the E-map. Full-matrix least squares / difference Fourier cycles were performed, which located the remaining non-hydrogen atoms. All non-hydrogen atoms were refined with anisotropic displacement parameters. The hydrogen atoms on the nitrogen were obtained via Fourier difference map and their positions were refined, and the rest of the hydrogen

atoms were placed in ideal positions and refined as riding atoms. The final full matrix least squares refinement converged to R1 = 0.0604 and wR2 = 0.1514 (F^2, all data).

Table S2. Crystal data and structure refinement for $[Co^{III}(DIM)(NO_2)_2]BPh_4$

Empirical formula	C36.50 H45 B1 Cl1 Co1 N6 O4	
Formula weight	736.99	
Crystal color, shape, size	red block, 0.250 x 0.200 x 0.100 mm^3	
Temperature	173 K	
Wavelength	0.71073 Å	
Crystal system, space group	Monoclinic, P 1 21/n 1	
Unit cell dimensions	a = 13.0529(7) Å	α= 90°.
	b = 25.0977(13) Å	β= 90.510(2)°.
	c = 21.7603(12) Å	γ = 90°.
Volume	7128.3(7) $Å^3$	
Z	8	
Density (calculated)	1.373 Mg/m^3	
Absorption coefficient	0.605 mm^{-1}	
F(000)	3096	
Data collection		
Diffractometer	Bruker Apex Kappa Duo, Bruker	
Theta range for data collection	1.239 to 26.475°.	
Index ranges	-16<=h<=16, -31<=k<=19, -27<=l<=26	
Reflections collected	43139	
Independent reflections	14446 [R(int) = 0.049]	
Observed Reflections	8819	
Completeness to theta = 25.151°	99.1 %	
Solution and Refinement		
Absorption correction	Semi-empirical from equivalents	
Max. and min. transmission	0.94 and 0.89	
Solution	Direct methods	
Refinement method	Full-matrix least-squares on F^2	
Weighting scheme	$w = [\sigma^2Fo^2 + AP^2 + BP]^{-1}$, with	
	$P = (Fo^2 + 2\,Fc^2)/3$, A = 0.045, B = 14.110	
Data / restraints / parameters	14385 / 20 / 908	
Goodness-of-fit on F^2	0.9861	
Final R indices [I>2sigma(I)]	R1 = 0.0604, wR2 = 0.1267	
R indices (all data)	R1 = 0.1101, wR2 = 0.1514	
Largest diff. peak and hole	1.38 and -1.26 $e.Å^{-3}$	

$Co^{II}(DIM)(NO_2)_2$

Data collection

A preliminary set of cell constants was calculated from reflections harvested from three sets of 12 frames. These initial sets of frames were oriented such that orthogonal wedges of reciprocal space were surveyed. This produced initial orientation matrices determined from 183 reflections. The data collection was carried out using Mo Kα radiation (graphite monochromator) with a frame time of 30 seconds and a detector distance of 4.0 cm. A randomly oriented region of reciprocal space was surveyed to achieve complete data with a redundancy of 4. Sections of frames were collected with 0.50º steps in ω and ϕ scans. Data to a resolution of 0.80 Å were considered in the reduction. Final cell constants were calculated from the xyz centroids of 3084 strong reflections from the actual data collection after integration (SAINT). The intensity data were corrected for absorption (SADABS).[36] Please refer to Table S3 for additional crystal and refinement information.

Structure solution and refinement

The space group $P2_1/c$ was determined based on intensity statistics and systematic absences. The structure was solved using Superflip[37] and refined (full-matrix-least squares) using the Oxford University Crystals for Windows system.[38] The charge-flipping solution provided most non-hydrogen atoms from the E-map. Full-matrix least squares / difference Fourier cycles were performed, which located the remaining non-hydrogen atoms. All non-hydrogen atoms were refined with anisotropic displacement parameters. The hydrogen atoms involved with hydrogen bonding were obtained from the Fourier difference map and their positions were refined, and the rest of the hydrogen atoms were placed in ideal positions and refined as riding atoms. The final full matrix least squares refinement converged to R1 = 0.0449 and wR2 = 0.1098 (F^2, all data).

Table S3. Crystal data and structure refinement for $Co^{II}(DIM)(NO_2)_2$.

Empirical formula	C12 H24 Co1 N6 O4	
Formula weight	375.29	
Crystal color, shape, size	black thick plate, 0.250 x 0.200 x 0.050 mm^3	
Temperature	173 K	
Wavelength	0.71073 Å	
Crystal system, space group	Monoclinic, $P2_1/c$	
Unit cell dimensions	a = 14.8094(6) Å	α= 90°.
	b = 8.3479(3) Å	β= 95.0227(12)°.
	c = 13.3835(6) Å	γ = 90°.
Volume	1648.21(12) $Å^3$	
Z	4	
Density (calculated)	1.512 Mg/m^3	
Absorption coefficient	1.070 mm^{-1}	
F(000)	788	
Data collection		
Diffractometer	Bruker Apex Kappa Duo, Bruker	
Theta range for data collection	2.761 to 26.375°.	
Index ranges	-18<=h<=18, -7<=k<=10, -16<=l<=16	
Reflections collected	11529	
Independent reflections	3319 [R(int) = 0.041]	
Observed Reflections	2497	
Completeness to theta = 25.056°	98.6 %	
Solution and Refinement		
Absorption correction	Semi-empirical from equivalents	
Max. and min. transmission	0.95 and 0.81	
Solution	Charge Flipping	
Refinement method	Full-matrix least-squares on F^2	
Weighting scheme	$w = [\sigma^2 Fo^2 + AP^2 + BP]^{-1}$, with	
	$P = (Fo^2 + 2\,Fc^2)/3$, A = 0.042, B = 2.980	
Data / restraints / parameters	3306 / 10 / 216	
Goodness-of-fit on F^2	0.9845	
Final R indices [I>2sigma(I)]	R1 = 0.0449, wR2 = 0.0985	
R indices (all data)	R1 = 0.0675, wR2 = 0.1098	
Largest diff. peak and hole	0.88 and -0.78 $e.Å^{-3}$	

References

1. Jackels, S. C.; Farmery, K.; Barefield, E. K.; Rose, N. J.; Busch, D. H., Tetragonal cobalt(III) complexes containing tetradentate macrocyclic amine ligands with different degrees of unsaturation. *Inorg. Chem.* **1972,** *11*, 2893.
2. Xu, S.; Ashley, D. C.; Kwon, H.-Y.; Ware, G. R.; Chen, C.-H.; Losovyj, Y.; Gao, X.; Jakubikova, E.; Smith, J. M., A flexible, redox-active macrocycle enables the electrocatalytic reduction of nitrate to ammonia by a cobalt complex. *Chem. Sci.* **2018,** *9*, 4950.
3. Baker, M. V.; Field, L. D.; Hambley, T. W., Diamagnetic paramagnetic equilibria in solutions of bis(dialkylphosphino)ethane complexes of iron. *Inorg. Chem.* **1988,** *27*, 2872.
4. Weatherburn, M. W., Phenol-hypochlorite reaction for determination of ammonia. *Anal. Chem.* **1967,** *39*, 971.
5. Frear, D. S.; Burrell, R. C., Spectrophotometric Method for Determining Hydroxylamine Reductase Activity in Higher Plants. *Anal. Chem.* **1955,** *27*, 1664.
6. Connelly, N. G.; Geiger, W. E., Chemical Redox Agents for Organometallic Chemistry. *Chem. Rev.* **1996,** *96*, 877.
7. Federico, F.; F., P. M.; Beatriz, R.; Julio, L. F., A Highly Active N-Heterocyclic Carbene Manganese(I) Complex for Selective Electrocatalytic CO2 Reduction to CO. *Angew. Chem. Int. Ed.* **2018,** *57*, 4603.
8. Barnett, S. M.; Goldberg, K. I.; Mayer, J. M., A soluble copper–bipyridine water-oxidation electrocatalyst. *Nat. Chem.* **2012,** *4*, 498.
9. Savéant, J.-M., Molecular Catalysis of Electrochemical Reactions. Mechanistic Aspects. *Chem. Rev.* **2008,** *108*, 2348.
10. Han, Y.; Wu, Y.; Lai, W.; Cao, R., Electrocatalytic Water Oxidation by a Water-Soluble Nickel Porphyrin Complex at Neutral pH with Low Overpotential. *Inorg. Chem.* **2015,** *54*, 5604.
11. Li, H. L.; Anderson, W. C.; Chambers, J. Q.; Hobbs, D. T., Electrocatalytic reduction of nitrate in sodium hydroxide solution in the presence of low-valent cobalt-cyclam species. *Inorg. Chem.* **1989,** *28*, 863.
12. Becke, A. D., Density-functional exchange-energy approximation with correct asymptotic behavior. *Phys. Rev. A* **1988,** *38*, 3098.
13. Lee, C.; Yang, W.; Parr, R. G., Development of the Colle-Salvetti correlation-energy formula into a functional of the electron density. *Phys. Rev. B* **1988,** *37*, 785.
14. Becke, A. D., Density-functional thermochemistry. III. The role of exact exchange. *J. Chem. Phys.* **1993,** *98*, 5648.
15. Becke, A. D., A new mixing of Hartree–Fock and local density-functional theories. *J. Chem. Phys.* **1993,** *98*, 1372.
16. Grimme, S., Semiempirical GGA-type density functional constructed with a long-range dispersion correction. *J. Comput. Chem.* **2006,** *27*, 1787.
17. Marenich, A. V.; Cramer, C. J.; Truhlar, D. G., Universal Solvation Model Based on Solute Electron Density and on a Continuum Model of the Solvent Defined by the Bulk Dielectric Constant and Atomic Surface Tensions. *J. Phys. Chem. B* **2009,** *113*, 6378.
18. Dolg, M.; Wedig, U.; Stoll, H.; Preuss, H., Energy-adjusted ab initio pseudopotentials for the first row transition elements. *J. Chem. Phys.* **1987,** *86*, 866.
19. Martin, J. M. L.; Sundermann, A., Correlation consistent valence basis sets for use with the Stuttgart–Dresden–Bonn relativistic effective core potentials: The atoms Ga–Kr and In–Xe. *J. Chem. Phys.* **2001,** *114*, 3408.

20. Peterson, K. A., Systematically convergent basis sets with relativistic pseudopotentials. I. Correlation consistent basis sets for the post-d group 13–15 elements. *J. Chem. Phys.* **2003,** *119*, 11099.
21. Hariharan, P. C.; Pople, J. A., The influence of polarization functions on molecular orbital hydrogenation energies. *Theor. Chim. Acta.* **1973,** *28*, 213.
22. Francl, M. M.; Pietro, W. J.; Hehre, W. J.; Binkley, J. S.; Gordon, M. S.; DeFrees, D. J.; Pople, J. A., Self-consistent molecular orbital methods. XXIII. A polarization-type basis set for second-row elements. *J. Chem. Phys.* **1982,** *77*, 3654.
23. Krishnan, R.; Binkley, J. S.; Seeger, R.; Pople, J. A., Self-consistent molecular orbital methods. XX. A basis set for correlated wave functions. *J. Chem. Phys.* **1980,** *72*, 650.
24. McLean, A. D.; Chandler, G. S., Contracted Gaussian basis sets for molecular calculations. I. Second row atoms, Z=11–18. *J. Chem. Phys.* **1980,** *72*, 5639.
25. Cramer, C. J., *Essentials of Computational Chemistry: Theories and Models.* 2nd ed.; John WIley & Sons: 2004.
26. Frisch, M. J.; Trucks, G. W.; Schlegel, H. B.; Scuseria, G. E.; Robb, M. A.; Cheeseman, J. R.; Scalmani, G.; Barone, V.; Mennucci, B.; Petersson, G. A.; Nakatsuji, H.; Caricato, M.; Li, X.; Hratchian, H. P.; Izmaylov, A. F.; Bloino, J.; Zheng, G.; Sonnenberg, J. L.; Hada, M.; Ehara, M.; Toyota, K.; Fukuda, R.; Hasegawa, J.; Ishida, M.; Nakajima, T.; Honda, Y.; Kitao, O.; Nakai, H.; Vreven, T.; Montgomery, J. A., Jr.; Peralta, J. E.; Ogliaro, F.; Bearpark, M.; Heyd, J. J.; Brothers, E.; Kudin, K. N.; Staroverov, V. N.; Kobayashi, R.; Normand, J.; Raghavachari, K.; Rendell, A.; Burant, J. C.; lyengar, S. S.; Tomasi, J.; Cossi, M.; Rega, N.; Millam, N. J.; Klene, M.; Knox, J. E.; Cross, J. B.; Bakken, V.; Adamo, C.; Jaramillo, J.; Gomperts, R.; Stratmann, R. E.; Yazyev, O.; Austin, A. J.; Cammi, R.; Pomelli, C.; Ochterski, J. W.; Martin, R. L.; Morokuma, K.; Zakrzewski, V. G.; Voth, G. A.; Salvador, P.; Dannenberg, J. J.; Dapprich, S.; Daniels, A. D.; Farkas, Ö.; Foresman, J. B.; Ortiz, J. V.; Cioslowski, J.; Fox, D. J. *Gaussian 09, Rev D.01*, Gaussian 09, revision D.01; Gaussian, Inc.: Willingford CT, 2009.
27. Kelly, C. P.; Cramer, C. J.; Truhlar, D. G., Aqueous Solvation Free Energies of Ions and Ion−Water Clusters Based on an Accurate Value for the Absolute Aqueous Solvation Free Energy of the Proton. *J. Phys. Chem. B* **2006,** *110*, 16066.
28. Kelly, C. P.; Cramer, C. J.; Truhlar, D. G., Single-Ion Solvation Free Energies and the Normal Hydrogen Electrode Potential in Methanol, Acetonitrile, and Dimethyl Sulfoxide. *J. Phys. Chem. B* **2007,** *111*, 408.
29. Fawcett, W. R., The Ionic Work Function and its Role in Estimating Absolute Electrode Potentials. *Langmuir* **2008,** *24*, 9868.
30. Tissandier, M. D.; Cowen, K. A.; Feng, W. Y.; Gundlach, E.; Cohen, M. H.; Earhart, A. D.; Coe, J. V.; Tuttle, T. R., The Proton's Absolute Aqueous Enthalpy and Gibbs Free Energy of Solvation from Cluster-Ion Solvation Data. *J. Phys. Chem. A* **1998,** *102*, 7787.
31. Zhan, C.-G.; Dixon, D. A., Absolute Hydration Free Energy of the Proton from First-Principles Electronic Structure Calculations. *J. Phys. Chem. A* **2001,** *105*, 11534.
32. Reiss, H.; Heller, A., The absolute potential of the standard hydrogen electrode: a new estimate. *J. Phys. Chem.* **1985,** *89*, 4207.
33. Bard, A. J.; Faulkner, L. R., *Electrochemical Methods: Fundamentals and Applications.* John Wiley & Sons: NY, 2000.
34. Harvey, J. N.; Aschi, M.; Schwarz, H.; Koch, W., The singlet and triplet states of phenyl cation. A hybrid approach for locating minimum energy crossing points between non-interacting potential energy surfaces. *Theor. Chem. Acc.* **1998,** *99*, 95.

35. SAINT, Bruker Analytical X-Ray Systems, Madison, WI, current version.
36. Blessing, R. H., An empirical correction for absorption anisotropy. *Acta Cryst. A* **1995,** *51*, 33.
37. Palatinus, L.; Chapuis, G., SUPERFLIP - a computer program for the solution of crystal structures by charge flipping in arbitrary dimensions. *J. Appl. Cryst.* **2007,** *40*, 786.
38. Betteridge, P. W.; Carruthers, J. R.; Cooper, R. I.; Prout, K.; Watkin, D. J., CRYSTALS version 12: software for guided crystal structure analysis. *J. Appl. Cryst.* **2003,** *36*, 1487.